IEEE Access
Multidisciplinary ⋮ Rapid Review ⋮ Open Access Journal

Received December 23, 2021, accepted January 1, 2022, date of publication January 4, 2022, date of current version January 13, 2022.

Digital Object Identifier 10.1109/ACCESS.2022.3140315

Torque Ripples Reduction and Performance Analysis of Electrically Excited Flux Switching Motor

BAKHTIAR KHAN, (Graduate Student Member, IEEE), FAISAL KHAN, (Member, IEEE), WASIQ ULLAH, (Graduate Student Member, IEEE), BASHARAT ULLAH, (Graduate Student Member, IEEE), AND SHAHID HUSSAIN, (Graduate Student Member, IEEE)

Department of Electrical and Computer Engineering, COMSATS University Islamabad, Abbottabad Campus, Abbottabad 22060, Pakistan

Corresponding author: Wasiq Ullah (wasiqullah014@gmail.com)

This work was supported in part by COMSATS University Islamabad, Abbottabad Campus, and in part by the Higher Education Commission of Pakistan under Grant TDF - 03 - 067/R&D/HEC/2019.

ABSTRACT Torque ripples cause acoustic noise, fluctuation in speed, vibration, and reduce lifetime of the motor. The double salient structure of Flux Switching Motor (FSM) has a high air-gap permeance variation that produces high torque ripples. This paper presents an analytical model to reduce air-gap permeance variation and torque ripples of the proposed octane modular stator 8slots-6poles single-phase Electrically Excited (EE) FSM. Furthermore, the rotor pole shaping technique is used to minimize the air-gap permeance variation and therefore, torque ripples of the proposed design are reduced. The electromagnetic performance of EEFSM is analyzed via the Finite Element Analysis (FEA) method. For the proposed design magnetic flux harmonics are reduced by 71% and back-EMF harmonics are suppressed by 48.5%. Torque ripples of the proposed EEFSM are reduced by 20%, cogging torque is diminished by 42.7% and average torque is enhanced by 5.8%. Finally, the prototype is fabricated and tested experimentally. Calculated values and experimental results are in good agreement and the difference is 3.5%-5%.

INDEX TERMS Torque ripples reduction, flux switching motor, single phase, electrically excited, analytical model, electromagnetic performance.

I. INTRODUCTION

The focus of research activities in advanced motors is high torque density, high power density, high efficiency, robust rotor structure, low noise and low cost [1]–[3]. Flux Switching Motors (FSMs) are attractive for their exclusive features [4]–[5]. Permanent Magnet (PM) FSMs have high torque density, high efficiency, simple and heavy-duty rotor construction [6]–[8]. However, PMFSM has disadvantages, e.g. it consumes rare-earth magnets and with the passage of time PM resources are depleting [9]–[13]. Moreover, the magnetic flux of PMFSM is uncontrollable and its performance is degraded with an increase in temperature [14], [15]. The magnetic flux of the Electrically Excited Flux Switching Motor (EEFSM) is controlled electronically, with an increase in temperature performance of EEFSM is not affected and its overall cost is low compared to the PMFSM. Single-phase EEFSM has many advantages i.e. its manufacturing process is simple, maintenance is easy, longer lifetime and low cost [3], [16].

Novel single-phase designs with good average torque and efficiency are presented in [16]–[18]. However, overlapped windings and segmented rotors are the drawbacks of these designs. Overlapped windings produce high copper losses and segmented rotors cannot be used for high-speed applications. In [19] all these concerns have been addressed but, the doubly salient structure of FSM is the cause of high air-gap permeance variation and torque ripples which produce acoustic noise, unwanted fluctuation in speed, vibration and reduce motor lifetime [20]. Comparative illustration of existing topologies is organized in Table 1.

In this paper, an analytical model and rotor pole shaping technique are presented for minimizing air-gap permeance variation and torque ripples of the octane modular stator EEFSM. The Copper Slot Filling Factor (CSFF) is calculated by an analytical method in [21] and octane modular stator

The associate editor coordinating the review of this manuscript and approving it for publication was R. K. Saket.

TABLE 1. Comparative Illustration of the Existing state of the art.

R.no.	Torque ripple	Rotor topology	Windings end effect
[16]	High	Segmented	Low
[17]	High	Salient	High
[18]	High	Salient	High
[19]	High	Salient	Low

EEFSM has 9% higher CSFF than the conventional designs. It has a salient pole rotor and can be used for high-speed applications [22]. The forward non-overlapped windings of the octane modular stator EEFSM has a low copper loss. Furthermore, it can be easily unfolded for coil placement, maintenance and transportation. For optimal performance of the proposed design, optimization is carried out. Besides, magnetic flux harmonics, back-EMF harmonics, cogging torque, torque ripples, average torque, output power, and efficiency of the proposed design are analyzed. Finally, the prototype is manufactured and tested experimentally.

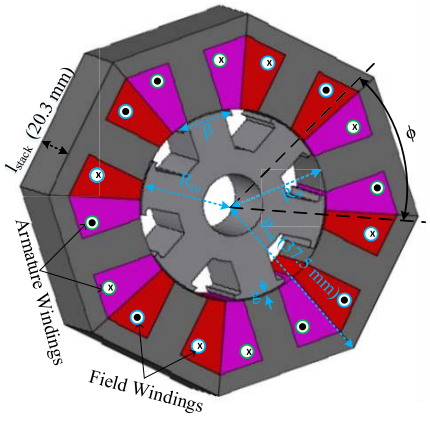

FIGURE 1. Octane modular stator 8S-6P single phase EEFSM geometrical representation.

II. PROPOSED TOPOLOGY AND ANALYTICAL MODEL

This section presents the proposed topology, analytical model for the reduction of permeance variation and torque ripples, and detailed discussion is included in the subsections.

A. PROPOSED TOPOLOGY

Figure 1 shows schematic of the proposed octane modular stator, rotor pole shaped rotor and forward non-overlapped windings. Fifty eight silicon steel sheets, each sheet of 0.35 mm are combined to get each T-shaped segment of octane modular stator and rotor pole shaped salient rotor.

B. ANALYTICAL MODEL

The doubly-slotted structure and main design parameters, i.e. internal radius of the stator (R_{si}), outer radius of the rotor (R_{ro}), air-gap (g), rotor displacement angle in the air-gap (ϕ) and rotor pole span (β) are given in Figure 1. The developed electromagnetic torque (τ) of EEFSM is given by [23]:

$$\tau = i_F i_A \frac{dL_{FA}}{d\theta} \tag{1}$$

where i_F, i_A, θ, L_{FA} are armature current, field current, rotor circumferential angle, mutual inductance of the field and armature windings, respectively. Also we can write electromagnetic torque as follows:

$$\tau = \tau_{avg} + \tau_{cog} \tag{2}$$

here τ_{avg} is the average torque of EEFSM and τ_{cog} is cogging torque produced due to energy variation in the motor parts. The energy variation in the air-gap is high due to the doubly-salient structure of EEFSM. This energy variation in the air-gap is minimum when the rotor poles aligned with the stator teeth and maximum while both are not overlapped. The cogging torque caused by energy variation in the air-gap is given as follows:

$$\tau_{cog} = \frac{\partial E_g}{\partial \theta} \tag{3}$$

Similarly, in terms of EEFSM parameters, energy in the air-gap (E_g) is calculated as follows [24]:

$$E_g = \frac{g^2 . l_{stack}}{4\mu_0} \int_0^{2\pi} B^2(\phi, \theta) . \Lambda^2(\Phi)\, d\phi \tag{4}$$

where μ_0, l_{stack}, $\Lambda(\phi)$ and $B(\phi, \theta)$ are permeability of free space, stack length of the EEFSM, permeance of air-gap and magnetic flux density, respectively. For 8s-6p EEFSM, $B^2(\phi, \theta)$ and $\Lambda^2(\Phi)$ fourier expansion is given as:

$$B^2(\phi, \theta) = \sum_{k=0}^{\infty} B_k \cos kT_s (\Phi + \theta) \tag{5}$$

T_s is number of stator teeth while B_k is air-gap flux density Fourier coefficient, and is given below:

$$\begin{aligned} B_k &= \frac{P_r}{\pi} \int_{-\gamma \frac{\pi}{P_r}}^{\gamma \frac{\pi}{P_r}} B_{max} \cos(M_L \theta) d\theta \\ &= \frac{2P_r}{k\pi M_L} B_{max} \sin(kM_L \gamma \frac{\pi}{P_r}) \end{aligned} \tag{6}$$

where γ is the ratio of rotor pole span and rotor pole pitch. EEFSM air-gap permeance model is presented in Figure 2 and permeance function is given below as:

$$\Lambda^2(\Phi) = \sum_{k=0}^{\infty} P_k \cos kP_r \Phi \tag{7}$$

P_r is the number of rotor poles and P_k air-gap permeance Fourier coefficient is given as follows:

$$\begin{aligned} P_k &= \frac{P_r}{\pi} \int_{\frac{\pi}{P_r} - \frac{\beta}{2}}^{\frac{\pi}{P_r} + \frac{\beta}{2}} \cos(kM_L \theta)\, d\theta \\ &= \frac{2P_r}{\pi k M_L} (-1)^{(k)(\frac{M_L}{P_r})} \sin(kM_L \frac{\beta}{2}) \end{aligned} \tag{8}$$

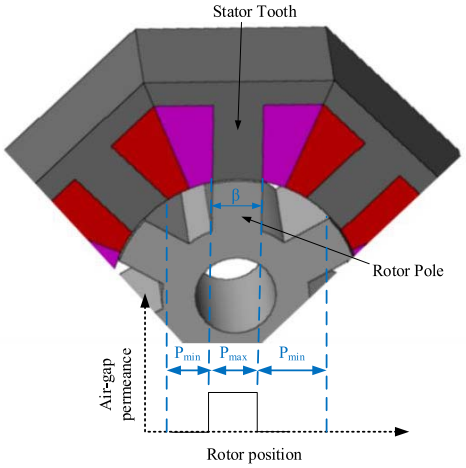

FIGURE 2. Octane modular stator EEFSM air-gap permeance model.

Putting (5) and (7) in (4), the energy in the air-gap is calculated. Further, by putting the result of (4) in (3) and by simplifying, cogging torque is formulated as:

$$\tau_{\text{cog}} = \frac{M_L \cdot \pi \cdot \text{g}^2 \cdot l_{stack}}{4\mu_0} \cdot \sum_{k=1}^{\infty} kP_k B_k \sin(kM_L\theta) \quad (9)$$

From (8) and permeance model in Figure 2, it is clear that air-gap permeance variation can be reduced by increasing the rotor pole span β, hence energy variation in the air-gap and thus overall ripples in the torque will be reduced.

The high variation in the air-gap permeance of the FSMs due to doubly-salient structure is the reason for torque ripples. These ripples can be reduced if the variation in the air-gap with the rotor rotation is minimized [25]. From (2) it can be seen that cogging torque (τ_{cog}) is the part of τ_{em}, however, τ_{cog} doesn't produce effective average torque and causes torque ripples [26]. If the variation in τ_{cog} is reduced, the overall variation in τ_{em} will be reduced. As permeance is reciprocal of reluctance, we can write τ_{cog} in terms of air-gap flux (φ_{g}) and variation of reluctance (R) in magnetic circuit with the rotation of the rotor [24] as:

$$\tau_{cog} = \varphi_{\text{g}}^2 \frac{d\text{R}}{d\phi} \quad (10)$$

When the stator tooth and rotor poles are not overlapped, flux goes through air-gap of high reluctance, compared to stator tooth and rotor poles overlapped. In this paper, rotor pole shaping technique is used for minimizing the reluctance variation and reduces toque ripples. Rotor Pole Shoe (RPS) dimensional parameters are shown in Figure 3 while the flux paths when stator and rotor pole are not overlapped are indicated in Figure 4. As in Figure 4, for simplicity the cylindrical coordinate θ is set out in linear coordinate manner as L and pole shoe height (S_h) is equal to pole shoe width (S_w). It is further assumed that flux lines are straight in air-gap region and circular elsewhere. The reluctance of the air-gap

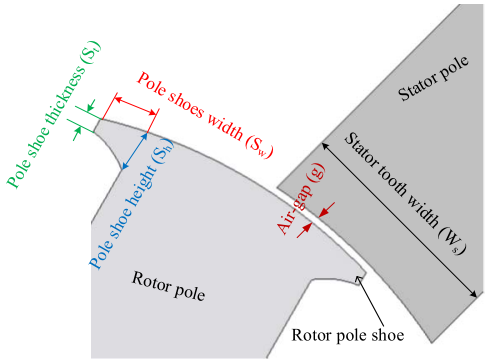

FIGURE 3. Rotor pole shoes dimensional design parameters.

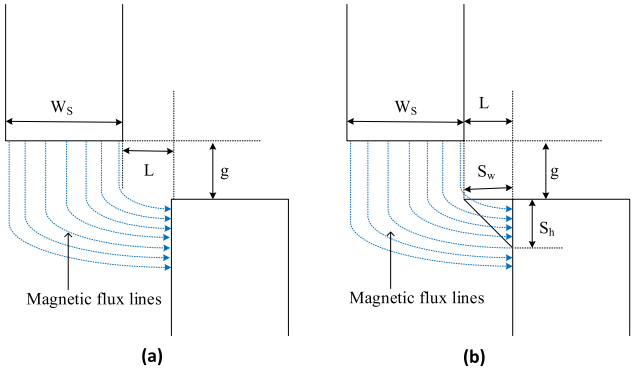

FIGURE 4. Magnetic flux paths model for non-overlapped stator tooth and rotor pole (a) without rotor pole shoe (b) with rotor pole shoe.

with rotor pole shoe is given as:

$$R = \frac{\pi}{2\mu_0 l_{stack} \ln\left[\left(\frac{\pi L+2g+\pi S_w}{\pi L+2g-\pi S_w}\right) \times \left(\frac{\pi L+2g+\pi W_S+\pi S_w}{\pi L+2g+2\pi S_w}\right)\right]} \quad (11)$$

by putting $\frac{dR}{dL} = 0$

Third order equation is obtained and by solving it, value of S_w is achieved in terms of W_s and g at any position L. Theoretically zero cogging torque can be calculated but practically it's not possible because the effect of magnetic saturation and flux leakage is not considered. The magnetic flux linkage distribution of octane modular stator EEFSM in Figure 5 shows that magnetic flux leakage is highly reduced with an increase in rotor pole span. For optimal performance, the analytical value of rotor pole shoe width and other parameters are optimized by using Finite Element Analysis (FEA) method.

III. PARAMETERS OPTIMIZATION

Deterministic Optimization (DO) is used to achieve the optimal values of RPS parameters. These parameters include Rotor Pole Shoe Width (RPSW), Rotor Pole Shoe Thickness (RPST) and Rotor Pole Shoe Height (RPSH). Magnetic Flux Harmonics (φ_h), back-EMF Harmonics (E_h), Cogging Torque (τ_{cog}), Instantaneous Torque (τ_{max} and τ_{min}), Torque Ripple (τ_{rip}) and Average Torque (τ_{avg}) are analyzed. Figure 6 presents the optimization procedure adopted in this paper while the pseudo code is given in Algorithm 1.

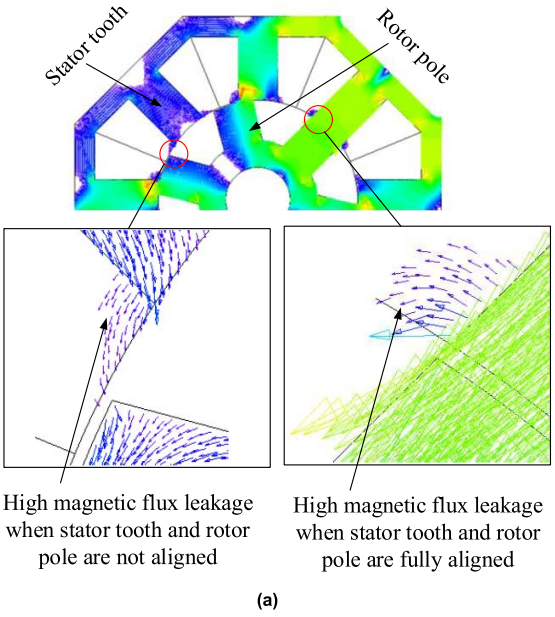

FIGURE 5. Magnetic flux distribution of octane modular stator EEFSM (a) conventional rotor (b) rotor pole shaped rotor.

The effect of each parameter variation on the performance of the proposed design is discussed in subsections.

Objective function, constraint and boundary condition are given as follows:

$$\begin{cases} \text{Objective function} \\ \min\left(\tau_{\text{cog}}\right) \\ \min\left(\tau_{\text{rip}}\right) \quad \text{and} \\ \max\left(\tau_{\text{avg}}\right) \end{cases}$$

$$\begin{cases} \text{Constraint} \\ \tau_{\text{rip}} < 0.845 \text{ N-m} \\ \tau_{\text{avg}} >= 0.48 \text{ N-m} \quad \text{and} \\ \tau_{\text{cog}} < 0.075 \text{ N-m} \end{cases}$$

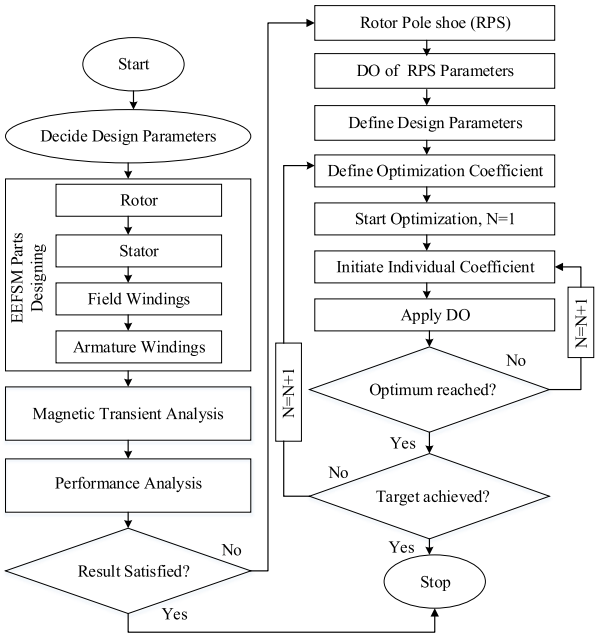

FIGURE 6. Flow chart for RPS parameters optimization.

Algorithm 1 Pseudo Code for RPS Optimization

Function $min\left(\tau_{cog}, \tau_{rip}\right), \max\left(\tau_{avg}\right)$
$\tau^*_{rip} = 0.845$ N-m, $\tau^*_{cog} = 0.075$ N-m, $\tau^*_{avg} = 0.48$ N-m
For $N = 1$ *to* N **do**
  if $S_w \geq 0$ & $S_w \leq 2$
    elseif $S_t \geq 0.25$ & $S_t \leq 1.5$
      elseif $S_h \geq 1$ & $S_h \leq 3$
        Calculate τ_{cog}
        Calculate τ_{rip}
        Calculate τ_{avg}
      end
    end
  end for
$\tau^*_{rip} = \tau_{rip}$
$\tau^*_{cog} = \tau_{cog}$
$\tau^*_{avg} = \tau_{avg}$
end function

$$\begin{cases} \text{Boundary condition} \\ 0 \leq S_w \leq 2 \\ 0.25 \leq S_t \leq 1.5 \\ 1 \leq S_h \leq 3 \end{cases}$$

A. EFFECT OF ROTOR POLE SHOE THICKNESS

Rotor Pole Shoe Width (RPSW) has major influence on the electromagnetic performance of the EEFSM, especially on φ_h, E_h, τ_{rip}, τ_{cog}, τ_{max}, τ_{min}, and τ_{avg}. RPSW is varied while RPST and RPSH are kept constant during the RPSW optimization. RPSW is varied 1-2mm and its effect on the key electromagnetic Performance Indicators (PIs) i.e. φ_h, E_h, τ_{cog}, τ_{max}, τ_{min}, τ_{rip} and τ_{avg} are organized in Table 2.

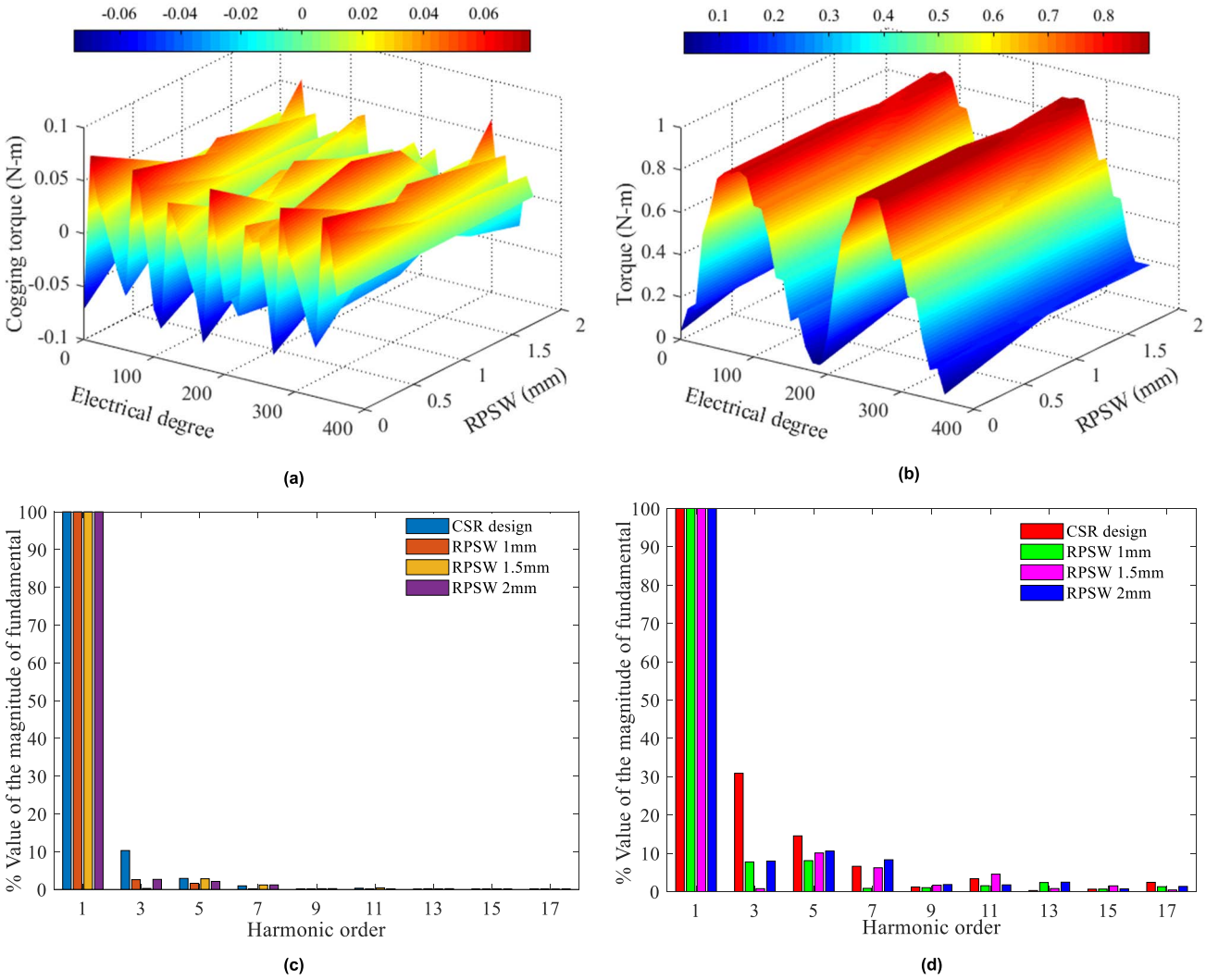

FIGURE 7. Effect of RPSW on (a) Cogging torque (b) Torque (c) magnetic Flux harmonics (d) Back-EMF harmonics.

TABLE 2. Effect of RPSW optimization on electromagnetic performance.

PIs	Unit	Initial Design	Optimized Design
φ_h	%	14.781	5.021
E_h	%	59.848	31.928
τ_{Cog}	N-m	0.075	0.047
τ_{max}	N-m	0.88	0.85
τ_{min}	N-m	0.035	0.157
τ_{rip}	N-m	0.845	0.693
τ_{avg}	N-m	0.48	0.514

Moreover, influence of RPSW variation on cogging torque, instantaneous torque, flux harmonics and back-EMF harmonics profile is plotted in Figure 7.

After RPSW optimization, φ_h is reduced by 66%, E_h is minimized by 46%, τ_{cog} is diminished by 37%, τ_{rip} are reduced by 18% and τ_{avg} is improved by 5%. The RPSW is updated to the optimized value of 1.5 mm.

B. EFFECT OF ROTOR POLE SHOE THICKNESS

In this subsection, the effect of Rotor Pole Shoe Thickness (RPST) variation on the electromagnetic performance of the EEFSM is analyzed. RPST is varied from 0.25 mm to 1.5 mm and its influence on PIs; φ_h, E_h, τ_{cog}, τ_{max}, τ_{min}, τ_{rip} and τ_{avg} are arranged in Table 3. Further, effect of RPST variation on cogging torque, instantaneous torque, flux harmonics and back-EMF harmonics profile is presented in Figure 8.

With RPST optimization φ_h decreased by 15%, E_h reduced by 3.6%, τ_{cog} minimized by 9%, τ_{avg} dropped by 1% and τ_{rip} reduced 2%. The RPST is updated from initial value 0.5 mm to optimized value 1 mm.

C. EFFECT OF ROTOR POLE SHOE HEIGHT

The influence of Rotor Pole Shoe Height (RPSH) on the electromagnetic performance of the EEFSM is investigated in this sub-section. RPSH is varied from 1 mm to 3 mm and its effect on φ_h, E_h, τ_{cog} and τ_{ins} is shown in Figure 9.

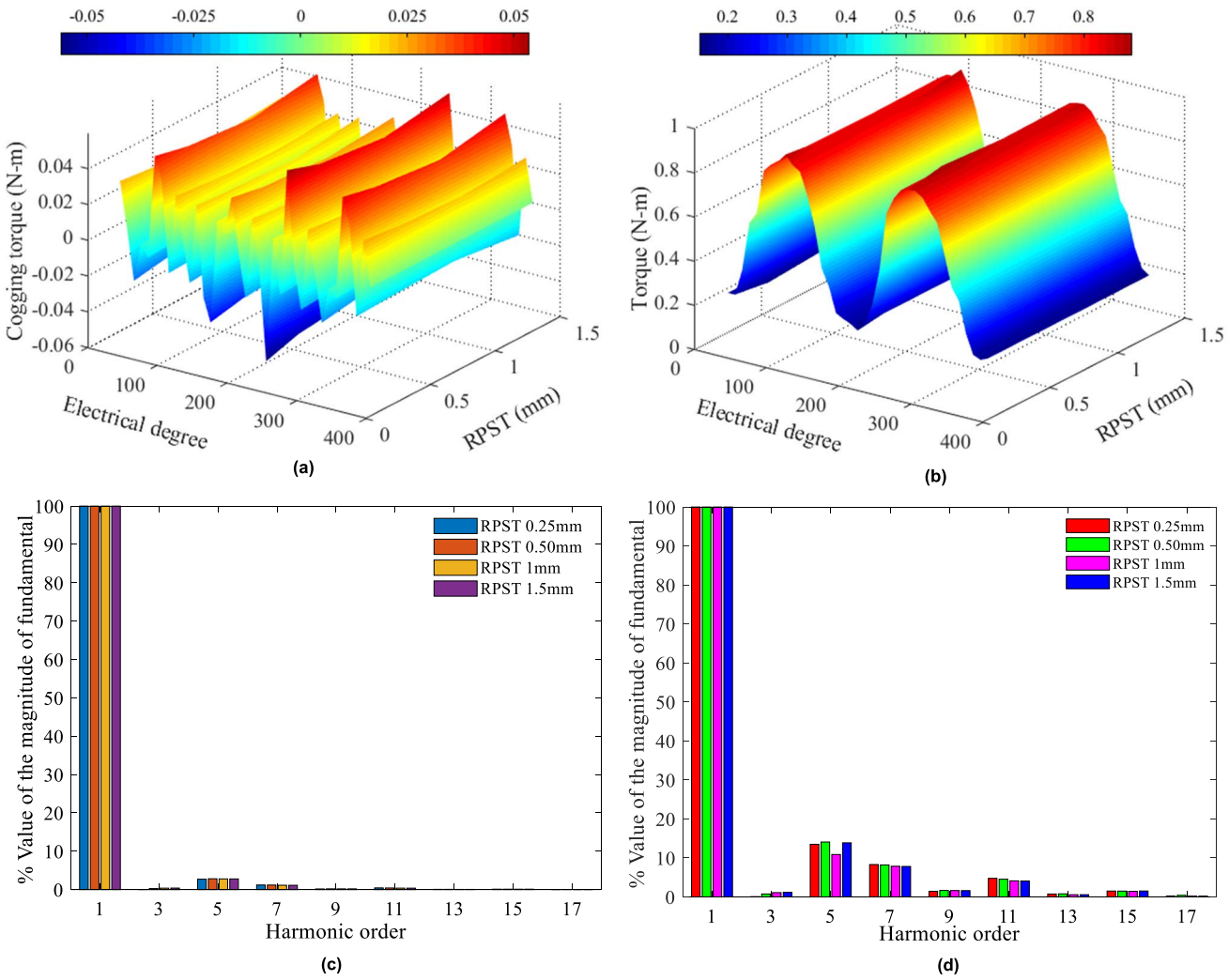

FIGURE 8. Effect of RPST on (a) Cogging torque (b) Torque (c) Magnetic flux harmonics (d) Back-EMF harmonics.

TABLE 3. Effect of RPST optimization on electromagnetic performance.

PIs	Unit	Initial Design	Optimized Design
φ_h	%	5.021	4.272
E_h	%	31.928	30.794
τ_{cog}	N-m	0.047	0.043
τ_{max}	N-m	0.85	0.848
τ_{min}	N-m	0.157	0.1635
τ_{rip}	N-m	0.693	0.6815
τ_{avg}	N-m	0.514	0.512

As RPSH is varied above and below the initial value of 1 mm, increase in magnetic flux harmonics, back-emf harmonics, cogging torque and torque ripples is observed. Therefore, RPSH is kept unchanged and 1 mm is taken as the optimal value.

IV. DISCUSSION

In this section, electromagnetic performance comparison is presented for the optimized design and conventional design. Further, φ_h, E_h, τ_{cog}, τ_{max}, τ_{min}, τ_{rip} and τ_{avg} are analyzed in the subsections.

A. MAGNETIC FLUX AND BACK-EMF HARMONICS ANALYSIS

The most important performance indicators magnetic flux and back-EMF are analyzed in this subsection. Magnetic flux and back-EMF harmonics of the conventional design and proposed design are plotted in Figure 10 and organized in Table 4. With overall optimization, magnetic flux harmonics for the proposed design are reduced by 71% and back-EMF harmonics are minimized by 48.5%.

B. COGGING TORQUE AND TORQUE RIPPLES ANALYSIS

Cogging torque is the cause of torque ripples, acoustic noise, vibration, unwanted fluctuation in speed and reduced lifetime

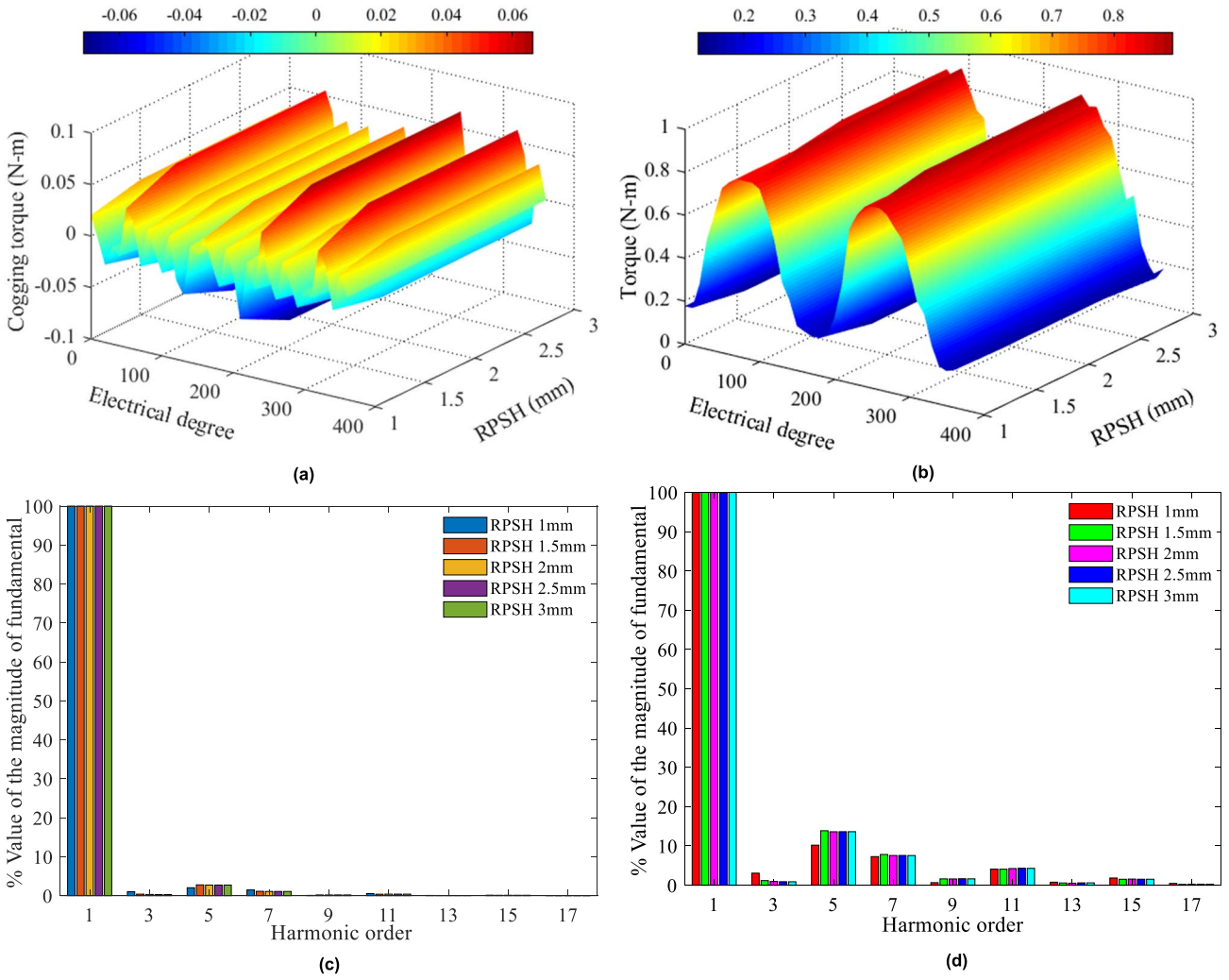

FIGURE 9. Effect of RPSH on (a) Cogging torque (b) Torque (c) Magnetic flux harmonics (d) Back-EMF harmonics.

TABLE 4. Electromagnetic performance comparison.

PIs	Unit	Conventional Design	Proposed Design
φ_h	%	14.781	4.271
E_h	%	59.848	30.794
τ_{cog}	N-m	0.075	0.043
τ_{max}	N-m	0.88	0.848
τ_{min}	N-m	0.035	0.1635
τ_{rip}	N-m	0.845	0.6815
τ_{avg}	N-m	0.48	0.512

of EEFSM [20]. Cogging torque for the proposed design and conventional design is plotted in Figure 11 (a) and arranged in Table 4. After RPS optimization, cogging torque for the proposed design is reduced by 42%.

Moreover, instantaneous torque plots for the proposed design and conventional design are given in Figure 11 (b). The maximum and minimum values are organized in Table 4. On the overall implementation of optimization process, the torque ripples of the proposed design are reduced by 20%.

C. TORQUE SPEED CHARACTRISTICS, OUTPUT POWER, LOSSES AND EFFICIENCY ANALYSIS

In this subsection, average torque, output power, iron loss, copper loss and efficiency are analyzed. Average torque and Output Power (P_o) versus speed are plotted in Figure 12 (a) while P_o, iron loss (P_i), copper loss (P_c) and efficiency are given in Figure 12 (b). Iron loss increased with increase in speed and at maximum speed of 14942.7 rpm, P_i is 8.89 Watts. Similarly, increase in armature current raised the copper loss and at $J_a = 15$ A/mm^2, P_c is recorded as 21.6 Watts. For the proposed octane modular stator EEFSM design, an average efficiency (η) of 89.5% is attained. An output power of 230 Watts under 0.512 N-m average torque and 4273 rpm medium speed at $J_e = 15$A/mm^2 & $J_a = 15$A/mm^2 is achieved, which is more suitable for

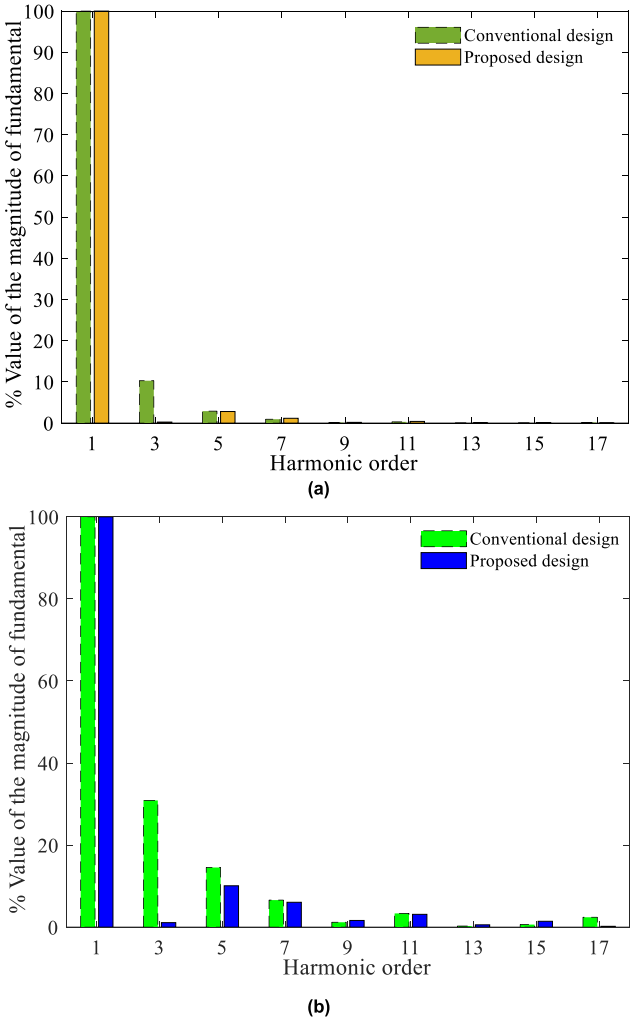

FIGURE 10. Harmonics comparison of conventional design and proposed design (a) Magnetic flux (b) Back-emf.

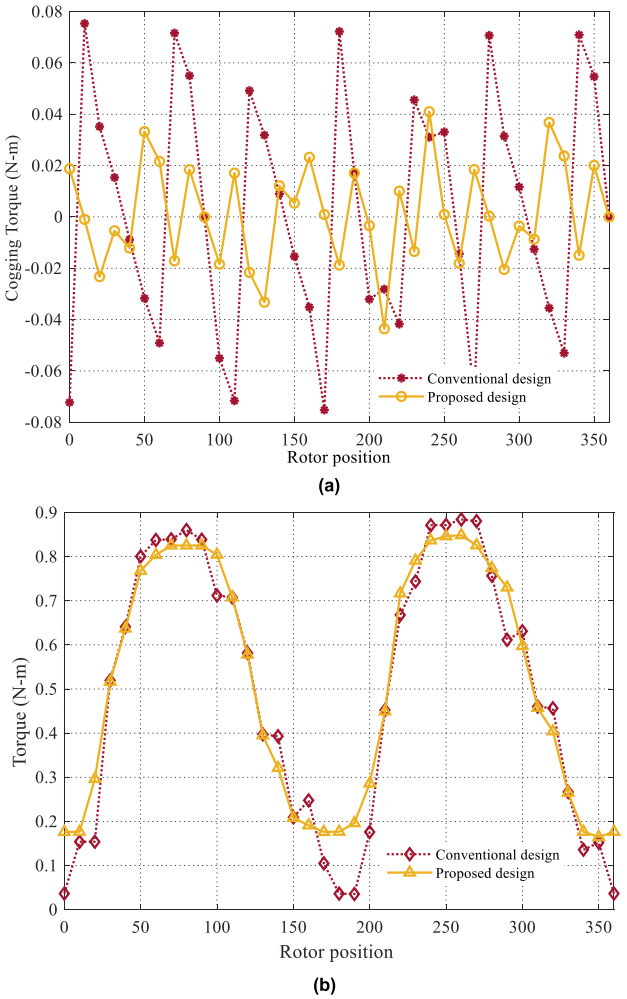

FIGURE 11. Cogging torque and torque comparison (a) Cogging torque at $J_e = 15$ (b) Instantaneous torque at $J_e = 15$ A/mm^2 and $J_a = 15$ A/mm^2.

TABLE 5. Performance Comparison.

PIs (Unit)	SegRN Design [16]	SalRN Design [19]	Proposed Design
φ_P (Wb)	0.026	0.0308	0.0310
E_h (%)	-	59.848	30.794
τ_{avg} (N-m)	0.30	0.48	0.512
τ_{rip} (N-m)	-	0.845	0.6815
P_{out} (Watts)	220	225	230
η (%)	73.5	91	89.5

home appliances. The proposed design has average torque 1.22 times and efficiency 1.24 times that of the conventional design in [16]. Furthermore, performance comparison of the proposed design, Segmented Rotor Non-overlapped (SegRN) design [16] and Salient Rotor Non-overlapped design [19] is presented in Table 5.

V. PROTOTYPE AND EXPERIMENTAL RESULTS

The manufactured octane modular stator EEFSM prototype main parts are presented in Figure 13. Figure 13 (a), (b), (c) and (d) show unfolded stator, folded stator with non-overlapped windings, rotor with RPS and complete motor assembly, respectively. For validation the basic principle of proposed design, the prototype is tested experimentally. Figure 14 shows the experimental test setup. This setup includes a test-bench, DC power source, AC power source, servo-motor, speed transducer, torque transducer, couplers, speed meter, torque meter, oscilloscope and digital multimeter.

To detect the presence of magnetic flux in the windings, no-load back-EMF test is performed at fixed speed of 500 rpm and various field current densities. The experimental no-load back-EMF results at various J_e are plotted in Figure 15(a). The no-load back-EMF profile follows a sinusoidal pattern and proved the basic principle of FSM. Moreover, at fixed $J_e = 15$ A/mm^2 the variation of no-load back-emf with the increase in speed is tested and presented in Figure 15(b). At low speed 500 rpm, peak value of back-emf is 11.96 V and

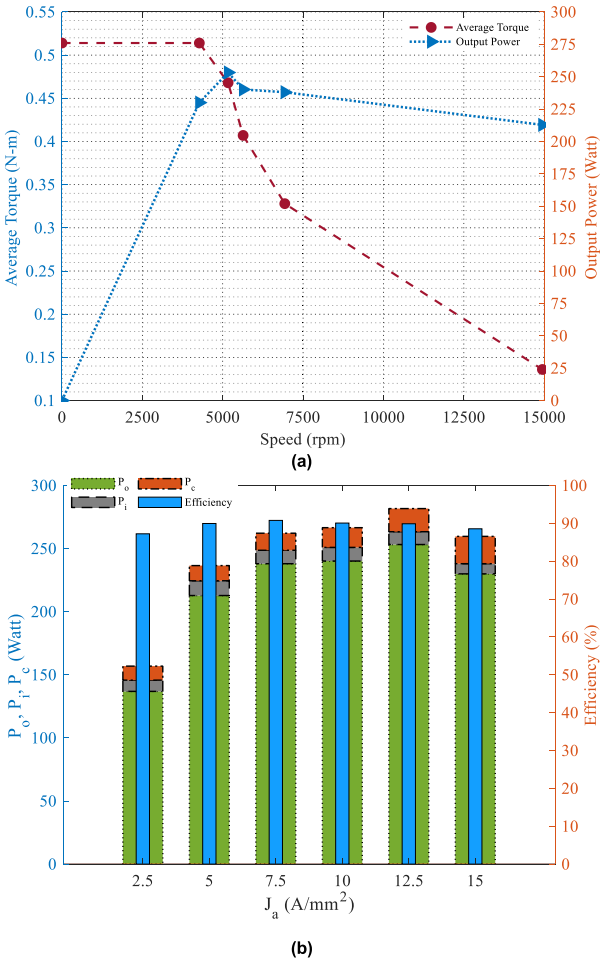

FIGURE 12. Proposed design (a) τ_{avg} and P_o versus speed (b) P_o, P_i, P_c and efficiency.

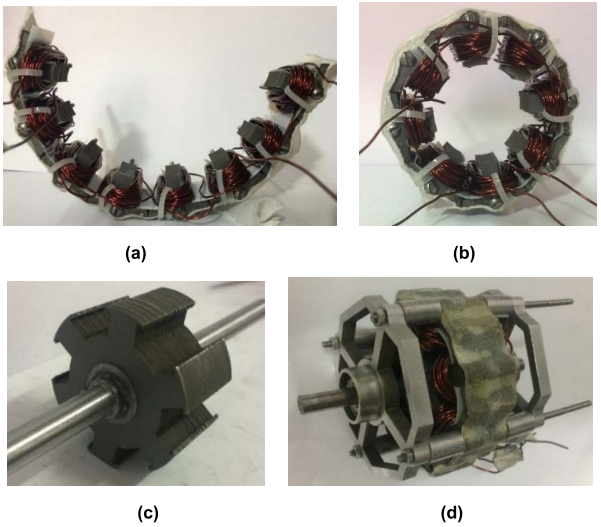

FIGURE 13. Prototype of the octane modular stator EEFSM (a) unfolded stator with windings (b) folded stator with windings (c) rotor with RPS (d) complete motor-assembly.

at high speed of 3000 rpm it is recorded as 71.77 V which is less than the supply voltage 220 volts and verifies motor principle.

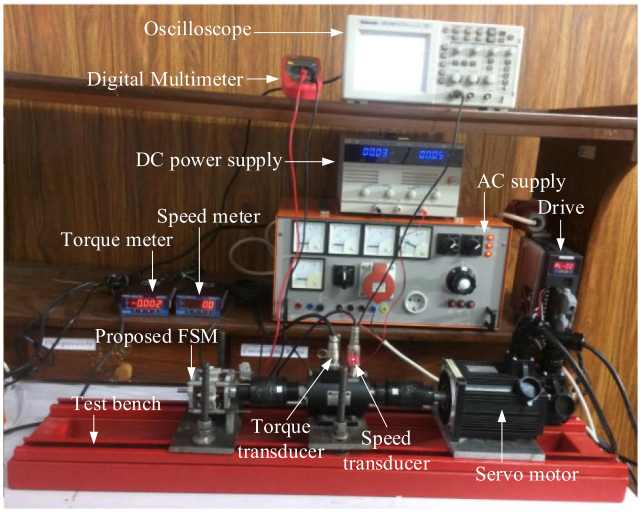

FIGURE 14. Experimental test setup.

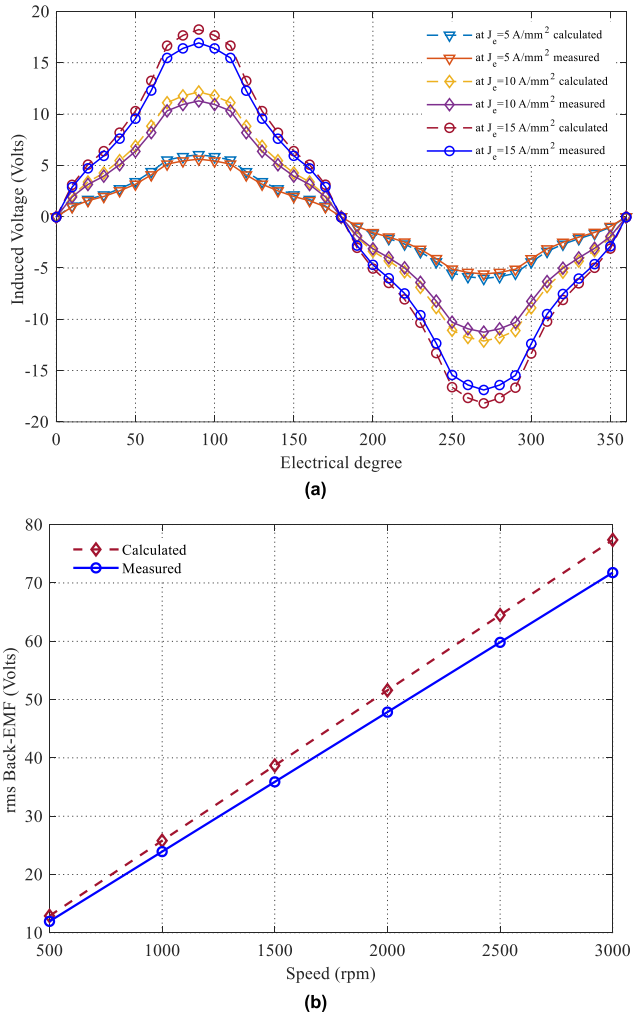

FIGURE 15. No-load test (a) Back-EMF profile at 500 rpm and different field current densities (b) Back-EMF versus speed and at J_e = 15 A/mm^2.

The effect of field current density (J_e) and armature current density (J_a) on average torque for the proposed octane

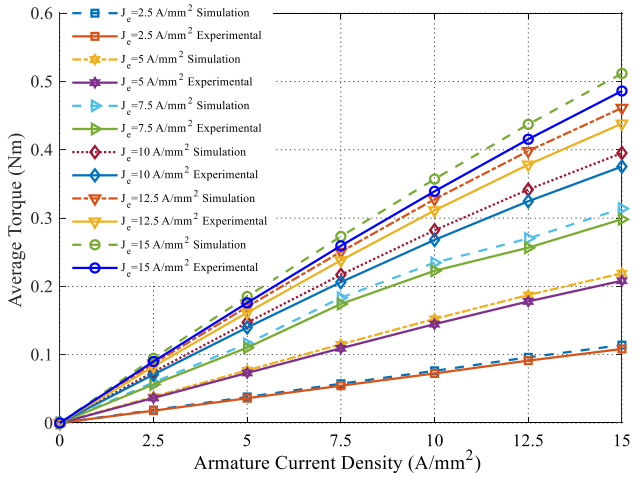

FIGURE 16. Proposed design load-test: Torque versus armature current density at various J_e and fixed 500 rpm.

modular stator EEFSM is tested and plotted in Figure 16. As the current density of the field windings and armature windings is increased, a proportional change in average torque is observed. At $J_e = 15$ A/mm^2 and $J_a = 15$ A/mm^2, an average of 0.482 N-m is recorded.

The experimental results are different from the calculated values. The cause of this variation is the copper wire tensile strength loss due to the manual motor windings process and ripples from DC power source [16].

VI. CONCLUSION

High torque ripples cause acoustic noise, unwanted fluctuation in speed, vibration and reduced lifetime of FSMs. Torque ripples are produced due to high air-gap permeance variation in the doubly-slotted geometry of FSMs. In this paper, analytical model was presented for the proposed octane modular stator EEFSM design to minimize air-gap permeance variation and therefore, reduce the torque ripples. Furthermore, the rotor pole shaping technique minimized the air-gap permeance variation and torque ripples. Moreover, the copper slot filling factor of the proposed design is higher than the conventional design and the copper losses are reduced by forward non-overlapped windings. For high speed cost sensitive applications its rotor is made salient pole. Besides, it can be unfolded for easy coil placement, maintenance and transportation. The magnetic flux harmonics of the proposed design are reduced by 71%, back-EMF harmonics are minimized by 48.5%. Similarly, cogging torque is diminished by 42%, torque ripples are reduced by 20% and average torque is improved by 5%. The average power of 230 Watts under 0.51 N-m is achieved. The proposed design has attained 89.5% average efficiency. The experimental results of the prototype have resemblance with the simulation results and difference is up to 5%.

REFERENCES

[1] I. Aghabali, J. Bauman, P. J. Kollmeyer, Y. Wang, B. Bilgin, and A. Emadi, "800-V electric vehicle powertrains: Review and analysis of benefits, challenges, and future trends," *IEEE Trans. Transport. Electrific.*, vol. 7, no. 3, pp. 927–948, Sep. 2021.

[2] H. Tu, H. Feng, S. Srdic, and S. Lukic, "Extreme fast charging of electric vehicles: A technology overview," *IEEE Trans. Transport. Electrific.*, vol. 5, no. 4, pp. 861–878, Dec. 2019.

[3] E. Bostanci, M. Moallem, A. Parsapour, and B. Fahimi, "Opportunities and challenges of switched reluctance motor drives for electric propulsion: A comparative study," *IEEE Trans. Transport. Electrific.*, vol. 3, no. 1, pp. 58–75, Mar. 2017.

[4] F. Zhang, X. Zhu, Z. Xiang, L. Quan, M. Jiang, S. Zheng, and D. Fan, "Low-loss-design of a flux-switching motor considering air-gap harmonics," *IEEE Trans. Appl. Supercond.*, vol. 30, no. 4, pp. 1–5, Jun. 2020.

[5] X. Sun, Z. Shi, G. Lei, Y. Guo, and J. Zhu, "Multi-objective design optimization of an IPMSM based on multilevel strategy," *IEEE Trans. Ind. Electron.*, vol. 68, no. 1, pp. 139–148, Jan. 2021.

[6] L. Mo, Z. Gangxu, T. Zhang, L. Qing, and L. Baolian, "Multilevel optimization design for a flux-concentrating permanent-magnet brushless machine considering PM demagnetization limitation," *IEEE Trans. Magn.*, vol. 57, no. 2, pp. 1–5, Feb. 2021.

[7] P. Su, W. Hua, M. Hu, Z. Wu, J. Si, Z. Chen, and M. Cheng, "Analysis of stator slots and rotor pole pairs combinations of rotor-permanent magnet flux-switching machines," *IEEE Trans. Ind. Electron.*, vol. 67, no. 2, pp. 906–918, Feb. 2020.

[8] W. Ullah, F. Khan, and M. Umair, "Lumped parameter magnetic equivalent circuit model for design of segmented PM consequent pole flux switching machine," *Eng. Comput.*, vol. 38, no. 2, pp. 572–585, Feb. 2021.

[9] Z. Q. Zhu and J. Chen, "Advanced flux-switching permanent magnet brushless machines," *IEEE Trans. Magn.*, vol. 46, no. 6, pp. 1447–1453, May 2010.

[10] X. Zhu, Z. Shu, L. Quan, Z. Xiang, and X. Pan, "Design and multicondition comparison of two outer-rotor flux-switching permanent-magnet motors for in-wheel traction applications," *IEEE Trans. Ind. Electron.*, vol. 64, no. 8, pp. 6137–6148, Aug. 2017.

[11] H. Yang, H. Lin, Z. Q. Zhu, D. Wang, S. Fang, and Y. Huang, "A variable-flux hybrid-PM switched-flux memory machine for EV/HEV applications," *IEEE Trans. Ind. Appl.*, vol. 52, no. 3, pp. 2203–2214, May/Jun. 2016.

[12] Z. Xiang, X. Zhu, L. Quan, and D. Fan, "Optimization design and analysis of a hybrid permanent magnet flux-switching motor with compound rotor configuration," *CES Trans. Electr. Mach. Syst.*, vol. 2, no. 2, pp. 200–206, Jun. 2018.

[13] Z. Z. Wu and Z. Q. Zhu, "Analysis of air-gap field modulation and magnetic gearing effects in switched flux permanent magnet machines," *IEEE Trans. Magn.*, vol. 51, no. 5, pp. 1–12, May 2015.

[14] F. Khan, E. Sulaiman, and Z. Ahmad, "Review of switched flux wound-field machines technology," *IETE Techn. Rev.*, vol. 34, no. 4, pp. 343–352, 2016.

[15] E. Sulaiman, T. Kosaka, and N. Matsui, "High power density design of 6-slot–8-pole hybrid excitation flux switching machine for hybrid electric vehicles," *IEEE Trans. Magn.*, vol. 47, no. 10, pp. 4453–4456, Oct. 2011.

[16] M. F. Omar, E. Sulaiman, M. Jenal, R. Kumar, and R. N. Firdaus, "Magnetic flux analysis of a new field-excitation flux switching motor using segmental rotor," *IEEE Trans. Magn.*, vol. 53, no. 11, pp. 1–4, Nov. 2017.

[17] Y. J. Zho and Z. Q. Zhu, "Comparison of low-cost single-phase wound-field switched-flux machines," *IEEE Trans. Ind. Appl.*, vol. 50, no. 5, pp. 3335–3345, Sep./Oct. 2014.

[18] J. Yuan, D. Meng, G. Lian, J. Zhang, H. Li, and F. Ban, "The stator slot-type optimization of electrical excitation flux-switching motor and its maximum torque/copper loss control," *IEEE Trans. Appl. Supercond.*, vol. 29, no. 2, pp. 1–5, Mar. 2019.

[19] B. Khan, F. Khan, W. Ullah, S. Hussain, and B. Ullah, "Analytical modelling, optimization and electromagnetic performance analysis of electrically excited flux switching motor," *IEEE Trans. Magn.*, early access, May 14, 2021, doi: 10.1109/TMAG.2021.3080292.

[20] E. I. Mbadiwe and E. B. Sulaiman, "Design and optimization of outer-rotor permanent magnet flux switching motor using transverse segmental rotor shape for automotive applications," *Ain Shams Eng. J.*, vol. 12, no. 1, pp. 507–516, Mar. 2021.

[21] B. Khan, F. Khan, W. Ullah, M. Umair, and S. Hussain, "Slot filling factor calculation and electromagnetic performance of single phase electrically excited flux switching motors," *Appl. Comput. Electromagn. Soc.*, vol. 35, no. 8, pp. 922–928, Oct. 2020.

[22] Z. Q. Zhu, Y. J. Zhou, J. T. Chen, and J. E. Green, "Investigation of nonoverlapping stator wound-field synchronous machines," *IEEE Trans. Energy Convers.*, vol. 30, no. 4, pp. 1420–1427, Dec. 2015.

[23] A. Zulu, B. C. Mecrow, and M. Armstrong, "A wound-field three-phase flux-switching synchronous motor with all excitation sources on the stator," *IEEE Trans. Ind. Appl.*, vol. 46, no. 6, pp. 2363–2371, Nov./Dec. 2010.
[24] S. E. Abdollahi and S. Vaez-Zadeh, "Reducing cogging torque in flux switching motors with segmented rotor," *IEEE Trans. Magn.*, vol. 49, no. 10, pp. 5304–5309, Oct. 2013.
[25] C. Sikder, I. Husain, and W. Ouyang, "Cogging torque reduction in flux-switching permanent-magnet machines by rotor pole shaping," *IEEE Trans. Ind. Appl.*, vol. 51, no. 5, pp. 3609–3619, Sep./Oct. 2015.
[26] J. Zhao, Y. S. Yan, B. Li, X. Liu, and Z. Chen, "Influence of different rotor teeth shapes on the performance of flux switching permanent magnet machines used for electric vehicles," *Energies*, vol. 7, no. 12, pp. 8056–8075, Dec. 2014.

BAKHTIAR KHAN (Graduate Student Member, IEEE) received the B.Sc. degree in electrical engineering from the University of Engineering & Technology, Peshawar, Pakistan, in 2007, and the M.S. degree in electrical engineering from COMSATS University Islamabad (CUI), Abbottabad Campus, Pakistan, in 2018, where he is currently pursuing the Ph.D. degree in electrical engineering. He is a member of the Electric Machine Design Research Laboratory, Department of Electrical and Computer Engineering, CUI. His research interests include design and analysis of flux switching machines for high-speed applications.

He is a member of Pakistan Engineering Council.

FAISAL KHAN (Member, IEEE) was born in Charsadda, Khyber Pakhtunkhwa, Pakistan, in 1986. He received the B.S. degree in electronics engineering and the M.S. degree in electrical engineering from COMSATS University Islamabad, Abbottabad Campus, Pakistan, in 2009 and 2012, respectively, and the Ph.D. degree in electrical engineering from Universiti Tun Hussein Onn Malaysia, Malaysia, in 2017.

From 2010 to 2012, he was a Lecturer with the University of Engineering & Technology, Abbottabad, Pakistan. Since 2017, he has been Assistant Professor with the Electrical and Computer Engineering Department, COMSATS University Islamabad. He is the author of more than 100 publications, one patent, and received multiple research awards. His research interests include design and analysis of flux-switching machines, synchronous machines, and DC machines.

Mr. Khan is a member of IEEE-IES Electrical Machines Technical Committee and a member of Pakistan Engineering Council.

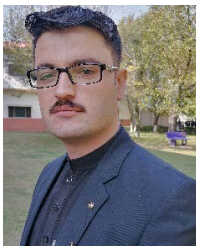

WASIQ ULLAH (Graduate Student Member, IEEE) was born in Peshawar, Khyber Pakhtunkhwa, Pakistan, in 1995. He received the B.S. and M.S. degrees in electrical (power) engineering from COMSATS University Islamabad, Abbottabad Campus, Abbottabad, Pakistan, in 2018 and 2020, respectively, where he is currently pursuing the Ph.D. degree in electrical (power) engineering.

Since 2018, he has been a Research Associate with the Electric Machine Design Research Laboratory. His research interests include analytical modeling, design analysis and optimization of permanent magnet flux switching machines, linear flux switching machines, hybrid excited flux switching machines, and novel consequent pole flux switching machines for high-speed brushless AC applications.

Mr. Ullah is basically from Afghanistan and serve as a Reviewer for IEEE Access, *IET Electric Power Application* and 2022 IEEE Energy Conversion Congress and Exposition (ECCE 2022). He is a member, an IEEE-IES Electrical Machines Technical Committee Members and a member of Pakistan Engineering Council.

BASHARAT ULLAH (Graduate Student Member, IEEE) received the B.S. degree in electronics engineering from the University of Engineering and Technology (UET), Peshawar, Pakistan, in 2015, and the M.S. degree in electrical engineering from the National University of Sciences and Technology (NUST), Islamabad, Pakistan, in 2017. He is currently pursuing the Ph.D. degree in electrical engineering from COMSATS University Islamabad, Abbottabad Campus. Since 2019, he has been a Research Associate with the Electric Machine Design Research Laboratory. His research interests include design, optimization and analysis of rotary and linear hybrid excited flux-switching machines, linear actuators, polyphase machines and their drives.

SHAHID HUSSAIN (Graduate Student Member, IEEE) was born in Swabi, Khyber Pakhtunkhwa, Pakistan. He received the B.S. degree in electrical (power) engineering from COMSATS University Islamabad, Abbottabad Campus, Abbottabad, Pakistan, in 2019. He is currently pursuing the M.S. degree in electrical (power) engineering. He has been a Research Assistant with the Electric Machine Design Research Laboratory, since 2020. His research interests include design analysis, optimization and experimental validation of modular and complementary fault tolerant field excited linear flux switching machines for long stroke application. He is a member of Pakistan Engineering Council.